Spring Semester Project Report

DUV Lithography for VHF resonators

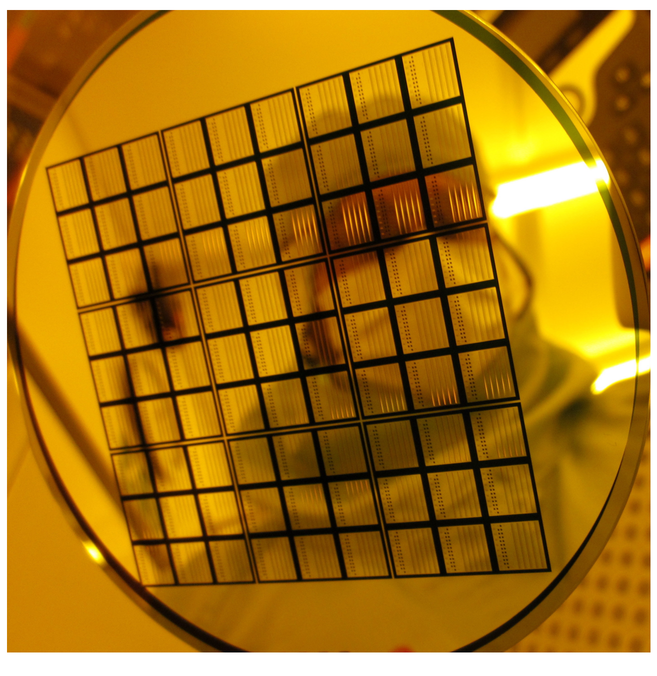

Advanced NEMS Laboratory - ANEMS

Professor:
Luis G. Villanueva

Author:
Pierre-Jean Croux

Supervisor:
Marco Liffredo

July 6, 2021

Acknowledgement

First, I would like to give a special thank to Marco Liffredo for his mentoring, precious advice and time spent answering my numerous questions.

In a second hand, to professor L.G. Villanueva and the ANEMS laboratory for giving me the opportunity to conduct this interesting project.

I also wanted to thank the CMi staff and especially N. Piacentini and J. Dorsaz for sharing their experience and for their disponibility to help me anytime. Finally, to M. Previde Massara from the Quack group for her precious answer on lift-off application.

Contents

1 Introduction **1**

2 Literature Review **2**
2.1 Contour-mode resonators CMRs 2
2.2 DUV Stepper lithography 3
2.2.1 Overview 3
2.2.2 Reticle Fabrication 3
2.2.3 Exposition 4
2.2.4 Materials 4
2.2.5 Computer optimisation 6
2.2.6 Comparaison with E-beam lithography 7
2.2.7 Lift-off application 7

3 Materials and Methods **9**
3.1 Overview 9
3.2 Mask design and fabrication 9
3.2.1 Pattern for reticle parameters optimization 10
3.2.2 Pattern for assessment of the lift-off and profile 11
3.3 Process Flows 12

4 Results and discussions **15**
4.1 Mask for reticle optimization 15
4.2 Final reticle fabrication 15
4.3 Results of wafer processing 16
4.3.1 First Batch: Wafer 1 & 2 17
4.3.2 Second Batch: Wafer 3 & 4 18
4.3.3 Third Batch: Wafer 5 & 6 23

5 Conclusion **24**

References **25**

A Process Flow 1 **28**

B Process Flow 2 **31**

C Table of measurements **34**

D Budget **35**

List of Figures

1 SEM picture of three CMRs operating at different frequencies . . . 1
2 LFE and TFE electrical configuration of CMRs . . . 2
3 Basic Photolithographic process . . . 3
4 Photomask fabrication process flow . . . 3
5 Wafer-Stepper scanner Schematic . . . 4
6 Relative Swing ratio of resist to Si . . . 6
7 Computer model output of resist profile and Mask OPC . . . 7
8 Applications of electron beam lithography . . . 7
9 LOR-PMGI Lift-off Process Flow . . . 8
10 Block diagramm of the project developpment . . . 9
11 CAD layout of the two main implemented patterns . . . 10
12 Mask layout for reticle optimization . . . 11
13 CAD layout of the final reticle chip . . . 12
14 Photoresist exposure and development schematic . . . 13
15 Surface activation and thin film metal deposition schematic . . . 13
16 Lift-off of the photoresist schematic . . . 14
17 SEM examination schematic . . . 14
18 Alternative process flow schematic . . . 14
19 Optimization results of the reticle fabrication using VPG200 . . . 15
20 Final reticle intensity dose mapping . . . 16
21 SEM pictures of damier and electrodes for wafer 1 . . . 17
22 Final wafer intensity dose mapping . . . 18
23 Remaining resist during liftoff for wafer 4 . . . 19
24 Critical Dimension inspection of damier feature for wafer 3 . . . 19
25 Over and underexposed chips comparison for wafer 3 . . . 20
26 VPG and stepper exposition parameters results for wafer 3 . . . 21
27 CD Bias parameters results for wafer 3 . . . 21
28 SEM pictures of the smallest achievable damier and electrode feature for wafer 3 22
29 SEM picture of the profile of a damier structure after cleaving for wafer 3 . . . 22
30 SEM pictures of the smallest achievable electrode feature for wafer 5 and 6 . . . 23

List of Tables

1 Fixed VPG200 parameters . . . 10
2 Photoresist coating and development parameters . . . 12
3 VPG paramters for the final reticle . . . 16
4 Wafers processing results resume . . . 17
5 Wafer 2 measurement results resume . . . 17
6 Resume of measurements made on the smallest achievable damier and electrode feature for wafer 3 . . . 22
7 Resume of measurements made on the smallest achievable electrode feature for wafer 5 and 6 . . . 23

1 Introduction

Micro and Nanoelectromechanical devices (MEMS & NEMS) have been of great interest in the domain of timing and filtering application for telecommunication. In particular, RF-Mems based front end represents a great solution following their small form factors, low power consumption and easy integration with CMOS circuits. In this project, we will focus on a particular type of device define as contour mode resonators (CMRs). They are piezoelectric resonant devices where the operating frequency can be tune by design. It enables thoses devices to have a large bandwitdh of operating frequencies from few MGHz up to GHz on the same silicon chip. They thus represent a competitive solution to traditional SAW, BAW pair and quartz crystal used for filters and oscillators. Research on CMRs resonators with diferents materials have already been conducted within the ANEMS laboratory, notably on wave lamb resonators and AINscn based oscillators and reflects the potential of such devices for application in modern telecommunication systems. The aim of this project is to optimise the fabrication of interdigitated electrodes array used in CMRs, which will be used as oscillator with an operating freqency capable of going to 2-4 GHz in order to address the requirements of the 5G industry. Closed loop oscillator are passive elements that cuts every frequencies out of the oscillating one and are thus used as reference fequency oscillators. The development process of designing new resonators is complex and necessits a rigurous assessment of the phase noise, a measure of the clock punctuality and intimately link to the quality factor [1] [2].

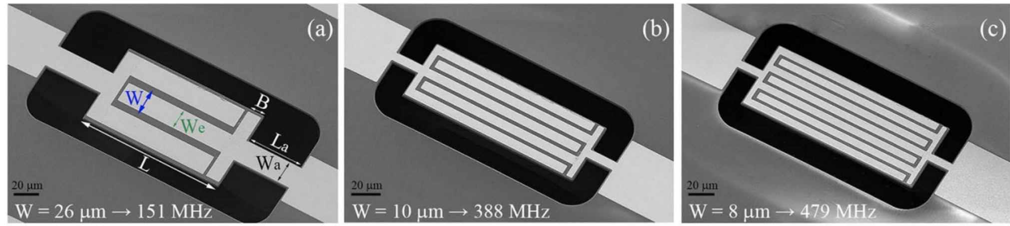

Figure 1: SEM picture of three CMRs operating at different frequencies [3]

Our approach is thus to scale down the design of CMRs electrodes array similar to the one illustrated in Figure 1 as a smaller pitch result to a smaller wavelength and therefore a higher frequency. The objective is to assess and optimize the feasability of IDT electrodes array with a resolution of 150 [nm] using DUV lithography, a technology which is more suited for industry manufacturing than E-beam lithography when comparing throughput of wafer, but also with a lower resolution limit and the requirements of having a reticle previously written. The project consist thus in two main steps:

- The optimization of the reticle using direct laser writing
- The optimization of exposure parameters in a ASML 5500 DUV Stepper

These two optimization steps will be done taking in consideration that the deposition of metal for the electrodes should be done by lift-off, but alternatives manufacturing solutions using DUV lithography will also be hrefly theoretically and experimentally investigate in order to compare the final achievable resolution of the designed patterns.

2 Literature Review

In this section, first strategies for the optimization of CMRs interdigitated electrodes array using DUV stepper lithography are reviewed.

2.1 Contour-mode resonators CMRs

Contour mode resonators are laterally vibrating microstructure based on piezoelectric material technology. They benefit from the unique feature of being able to choose the operating frequency over a wide spectrum by tuning a simple design parameter. As well as other resonators, their resonant frequency is intimately linked to its Q factor number which is defined in equation 2.1 [4].

$$Q = \frac{f_0}{BW_{3dB}} \tag{2.1}$$

It is important to note that by definition, increasing the Q factor is equivalent to having more energy stored at the resonant frequency. For CMRs, the energy losses come either from material properties or from design, which can be tuned in order to optimise the resonator and thus the resonant frequency. We highlighted three main categorizes of energy losses to better understand this concept.

- Electrical energy losses
- Material losses
- Acoustic losses in the substrate

The latter is directly linked to the confine energy on the substrate. This acoustic energy can thus be optimised by design and represents a good solution to increase the resonant frequency. CMRs bring the possibility of tuning the frequency via design and they also have great characteristics in term of performances such as a high quality factor over 1000 in the air, motional resistance of the range of 25-250 [Ω] and good capacitance value parameter. In addition, CMRs offer the unique feature to be able to design multiple frequencies on the same chip. All those aspects make of CMRs a very appealing solutions for the new wireless communication generation, especially as timer and filters for RF front ends from few MHz to GHz [5].

Figure 2: LFE and TFE electrical configuration of CMRs [4]

Figure 2 illustrates the two possible configurations for CMR resonator: thickness field excitation (TFE) and lateral field excitation (LFE). We will focus on the latter which is constituted of a bottom plate electrode electrically floating, on which there is a layer of piezoelectric material. Finally, the top electrode is designed to be an interdigital transducer (IDT). The application of an electric field excite the lateral, so called contour mode, following electromechanical conversion. The resonant frequency is thus proportional to the pitch of the IDT electrodes, as decreasing the pitch will lead to a higher operating frequency.

2.2 DUV Stepper lithography

2.2.1 Overview

Photolithography is the process by wich a pattern is defined into a photoresist through a photomask using the illumination of light at a specific wavelength. This process is widely porformed in the production of circuits board and discrete electronic devices. The basic process of photolithography is shown in Figure 3.

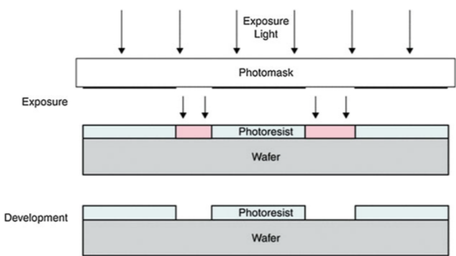

Figure 3: Basic Photolithographic process [6]

The nature of the photoresist can be called positive or negative which will change it's response to the illumination. In this case, a positive photoresist is previouly coated on the substrate, then the exposition will enhance a chemical change that will allow the illuminated resist to be removed by a developer in order to create the wanted pattern. The photomask is normally made of chromium and soda lime glass for typical UV lithography.

Deep Ultraviolet Photolithography is the process by which a pattern is defined into a photoresist using 254-193 [nm] light. The photosensitive polymer layer pattern is exposed through a chrome-on-quartz reticle using stepper technology. The main difference for the photomask is that for typical UV lithography, the photomask is applied using hard contact on the wafer and for DUV lithography, using a stepper, hence the necessity of using quartz instead of glass.

2.2.2 Reticle Fabrication

The main process of reticle fabrication is shown in Figure 4.

Figure 4: Photomask fabrication process flow

Maskless lithography (MLP) is used to pattern the resist coated on top of the mask. Various techniques are used such as E-beam or optical MLP [7]. In our case, an UV laser beam at 355 [nm] is focused over the substrate and illuminate the resist by direct exposure. note that this equipment is optimised for very high-speed pattern generation. The chromium is then etch using dry chemistery and finally, the resist is stripped. The pattern is inverted as the chromium part of the mask will be facing downward during illumination to minimize the effects of diffraction. The resolution of the equipment used for the fabrication of the Mask is a great challenge when patterning reticle for nanoscale on-wafer dimension. As the resolution is limited by the photoresist, wavelength and resolving power of the optics, the need for other fabrication solutions has to be taken into consideration such as professional mask manufacturer.

2.2.3 Exposition

The main schematic of DUV lithography using a stepper is shown in Figure 5, it is based on the utilization of a demagnifying lense between the Mask and the substrate [8] [9].

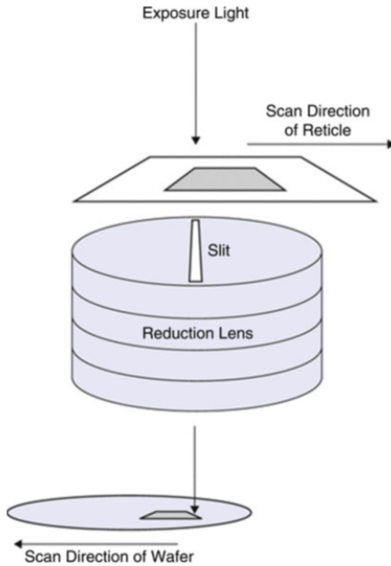

Figure 5: Wafer-Stepper scanner Schematic [6]

As shown in Figure 5, in the case of DUV lithography, a reduction lens is used to reduce the critical dimension of the pattern of the reticle four times at the wafer level. The stepper being an exposure system, the resolution of narrow lines exposed through a reduction lens is calculated based on the Rayleigh criterion [10].

$$R = k_1 \frac{\lambda}{NA} \tag{2.2}$$

With R, the resolution of the system defined as half of the smallest printable pitch, λ is the wavelength of the exposure light, NA is the numerical aperture of the lens and k_1 is a process-dependent factor.

Based on equation 2.2, it is trivial that a smaller wavelength will lead to a smaller critical dimension at the scale of the printed wafer, which reassure the principle of using deep UV light for lithography with the purpose of even greater miniaturization of Integrated Circuits.

Another important parameter to take in consideration for such systems and considering the application of photoresist exposure is the depth of focus of the exposition tool, defined similarly as equation 2.2.

$$DOF = k_2 \frac{\lambda}{NA^2} \tag{2.3}$$

With DOF being the depth of focus and k_2 is another process-dependant factor. The depth of focus represents the vertical distance over which the image remains in focus and is one of the most important parameters that limit the process latitude. We are thus confronting a trade-off of technology when lowering the illumination wavelength to produce smaller feature as we want to decrease the resolution by keeping a good depth of focus.

2.2.4 Materials

The conclusion coming from the above section lead to an important consideration of the possible material that can be process. In order to enable patterning with a resolution lower than 200

nm, the ASML PAS 5500/350C Stepper available in the Cmi use a lens with high numerical aperture tunable from 0.5 to 0.7 and a KrF laser source producing a 248 [nm] light [11]. The needs for such illumination parameters also limit the depth of focus to an approximated value of 1 [μm]. In other words, if the wafer surface is further away than $\pm$ 500 [nm] from the defined plane of focus, the quality of the printed pattern will be particularly deteriorate. Thus, to optimise the critical dimension uniformity (CDU) taking into consideration the properties of projection optics there is a special flatness requirement over the wafer substrate being 2 [μm] TTV for the least rigourous process and 0.5 [μm] TTV for many critical application [6].

Photoresist

The breakthrough that led to the development of DUV lithography was the successful research conducted by IBM, Frechet, Willson and Ito in the early 1980s on chemically amplified photoresist. Indeed, the reduction in the wavelength of the illuminating source also lowered its intensity. To enable DUV lithography process, photoresist with a higher sensitivity were needed to counter the loss in intensity [12].

For typical industrial application with 248 [nm] light, the chemical amplification is based on acid-catalyzed mechanism. The main component is a polymeric matrix containing most of the propoerties of the photoresist film. Added to that, there is photoacid-generator molecules (PAGs) that will enhance the sensitivity to ultraviolet light and finally it is also composed of base quencher molecules that acts as dissolution inhibitor and provide solubility switch before and after exposure. This complex method of multiplication of acid formed by exposure leads to a greater sensitivity of DUV resist up to several orders of magnitude.

Prior exposition, the dissolution inhibitor, which are acid-labile protecting group, totally prevent the dissolution of the resist. Then, following exposition, acids are generated and attacks the protecting group, leading to an acid-catalized deprotection reaction. The change in dissolution rate of the matrix is then reverse by applying a post-exposure bake (PEB). It is thus very important to consider that during the time following exposition and before PEB, the resist continues to "developp herself" at a rate of around 1-2 [nm] per minutes for resist available in the CMi [13] [14].

In addition to this new resist technology enabling lithography at deep UV level, DUV lithography has another advantage over standard UV as it permits to achieve a better resolution following equation 2.2. Indeed, the k_1 factor, which is empirically defined is much smaller for DUV than for UV. However, the DOF limitation implies to use much smaller photoresist thickness in order to stay in the available focus latitude and achieve uniform exposition.

Finally, researchs in this area continue evolving with the development of highly sensitive resist for Extreme Ultraviolet (EUV) lithography with greatly enhance performances based on the same chemical amplification mechanism. EUV lithography represents the next lithography generation with a light emission source at 13.5 [nm] that will help to scale down even-more the resolution limit of the semi-conductor industry [15].

Process optimisation layer

Another challenging parameter that needs to be taken into consideration is the reflection of radiation from the substrate back to the photoresist layer. At the DUV scale, the photoresists used are particularly transparent and the substrate and photoresist reflectivity are also greater compare to standard UV. Thus, the tiny change in optical phase happening due to thin film interference can lead to considerable change in exposure dose. Following a simple optical model of photoresist, a measure for film thickness induced change of photoresist is expressed and define as the Swing ratio S.

$$S = 4\sqrt{R_r R_s} e^{-\alpha D} \tag{2.4}$$

Where R_r and R_s are the reflectivity at respectively the interface resist-air and substrate-resist. D is the resist film thickness and α is the resist absortion. Several resist process have been developed in order to increase control over this parameter such as Top Surface Imaging (TSI), dyed resist which increase the absortion, Top Anti reflective Layer (TARC) and more commonly, Bottom Anti Reflective Layer (BARC), which lower the R_s coefficient and minimize the Swing ratio number [16].

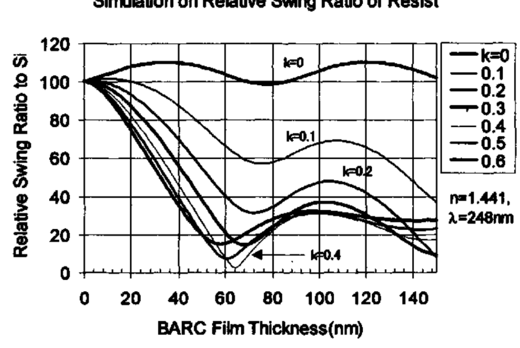

Figure 6: Relative Swing ratio of resist to Si [17]

The BARC layer needs to be applied between the substrate and the resist at a particular optimised thickness in order to reduce the reflectivity coefficient. As a proof of concept, Figure 6 shows the PROLITH simulation of optimum BARC condition for various k value, which represents the imaginary part of the BARC refractive index at 248 [nm] and depends on the absorbtion coefficient. We can see that BARC application can greatly minimize the Swing Ratio for a particular thickness that needs to be optimised prior exposition using a simulation software and thus lead to better imaging control. However, conventional BARC are not applicable in every application, since the removal of this anti-reflective layer often necessits a dry etch step after the development of the photoresist, which add another step along to the coating of the BARC. On the other hand, the use of BARC acts as an adhesion layer for the photoresist to the surface and reduce the need of priming [17].

2.2.5 Computer optimisation

Another possibility that has been investigated in order to have more control over the pattern and optimise processing parameters is computer modeling. The modelisation of the pattern can save considerable effort on the DUV stepper tool which can be very expensive for the development of a project. Parameters such as the dose, focus and illuminations settings can be set prior starting experimentation. Particularly, the role of Optical Proximity Correction which is illustrated in Figure 7 has been shown to have great results in order to bring lithography generated pattern as close to the desired target pattern as possible [18] [19].

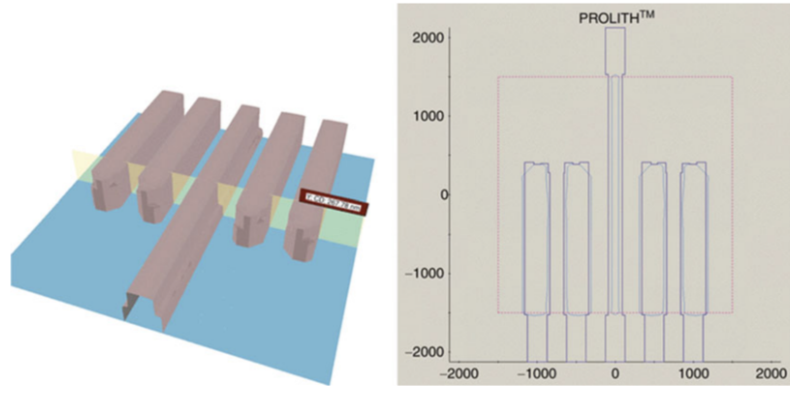

Figure 7: Computer model output of resist profile and Mask OPC [6]

2.2.6 Comparaison with E-beam lithography

In the event where we need to manufacture smaller feature for the IC industry at the nanoscale using lithogrpahy, two main methods are taken into account in this project. The previously mentionned DUV stepper lithography and the E-beam lithography. E-beam lithography resolution can come down to 0.1 nm and images in the range of 3-8 nm are achievable in resist, a feature size that is not at all already achievable with actual DUV stepper techniques. However, writing speeds limits the throughput of this technology and thus increase the cost in volume manufacturing.

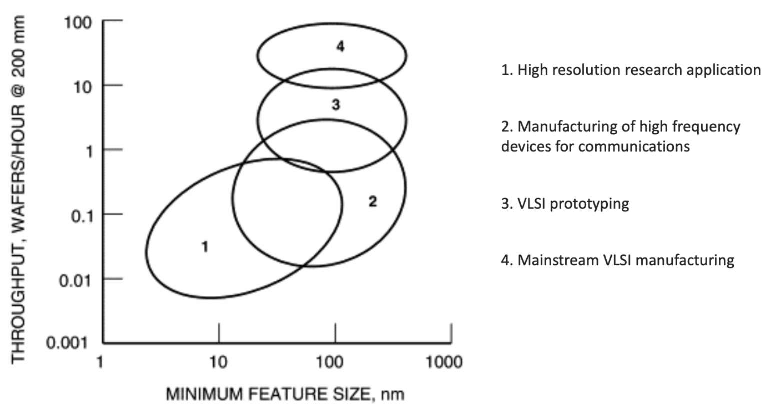

Figure 8: Applications of electron beam lithography, plotted as a function of minimum linewidth (horizontal axis), and throughput (vertical axis) [20]

As we can see in Figure 8, the throughput for our application is very low compare to DUV stepper lithography that can process more than 100 wafers per hour. Stepper lithography represents thus a more suitable solutions for industry, at the expand of having to manufacture a reticle and a complex exposition parameters optimization when coming close to the critical resolution of this technology.

2.2.7 Lift-off application

A lift-off is the process of patterning a target material on a substrate using a sacrificial material. In our case, the sacrificial material is the photoresist and its stripping allows the creation of structure. It represents an alternative to etching of a material. However, achieving consistent lift-off for critical nonascale dimensions represents a great challenge as defects can come from

photolithography, metal deposition or resist removal and can fail the process. Effectively, in order to optimise the lift-off sucess, undercut resist profile are preferred as well as anisotrope metal deposition. The first one represents a great challenge in DUV stepper lithography as it is limited by the optics parameters and notably the previously mentioned depth of focus. However, some application found alternative to simple resist exposition for more successfull lift-off that could be of great inspiration for future work on this project and are briefly presented below [21].

Multilayer lift-off

Different alternatives for lift-off with multilayer have been developped in order to enhance the undercut of the resist and achieve lift-off with a greater success rate. In particular, LOR and PMGI resist have been designed to enable sub 250 [nm] patterning with an excellent adhesion to Si. The schematic utilization of those resists is presented in Figure 9

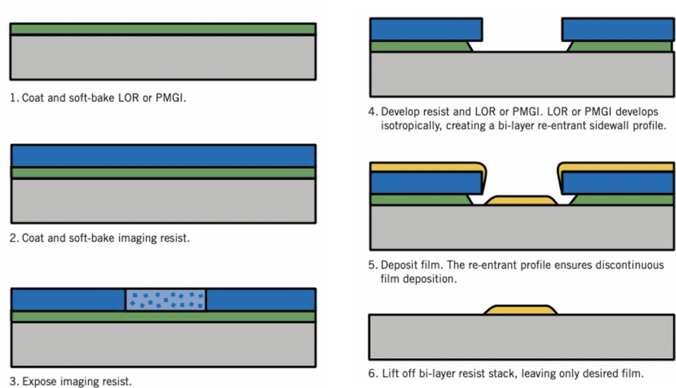

Figure 9: LOR-PMGI Lift-off Process Flow [22]

Typically, the thickness of the resist should be bigger than the deposited metal one. Also note that the exposed resist is only the imaging one and that the isotropic developement of LOR-PMGI resist thus enable bi-layer re-entrant sidewall profile.

Studies about the manufacture of developable BARC (DBARC) proposed by Cameron and al. [23] also opens the door to new challenging lift-off process by enalbling the possibility of using BARC layer in this process.

Nanoimprint Stepper lithography

In this section, an alternative to DUV lithography patterning for lift-off application exposed by Tallal and al. demonstrated the feasibilitry of reliable 250 nm wide metallic pattern lift-off using trilayer nanoimprint lithography (LIT). NIL isn't constrain by the optical diffraction limit but has the inconvenience of having to manufacture the needed mold. This trade-off actually make of NIL a high-throughput and reasonable cost solution to DUV lithography for patterning of nanoscale structures for the industry [24] [25].

3 Materials and Methods

3.1 Overview

In the scope of this project, we want to assess the feasability of a lift-off process for the manufacture of IDT fingers with pitch down to 150 [nm] using deep UV lithography technology. We based our development on available materials and equipments at the center of MicroNanoTechnology (CMi) at EPFL. Following conclusion of the literature review and after investigation of possible process we conclude that using BARC layer was not suitable for this lift-off application as we don't have access to Developable BARC, multilayer lift-off in not conceivable with CMi ressources, mainly due to the complexity in processing that it implies and the high sensitivity of the stepper to outside contamination. However, OPC could represents an implementable solution for better mask patterning and we highly recommand its investigation in further step of this project. The main block diagramm of the project development is shown in figure 10.

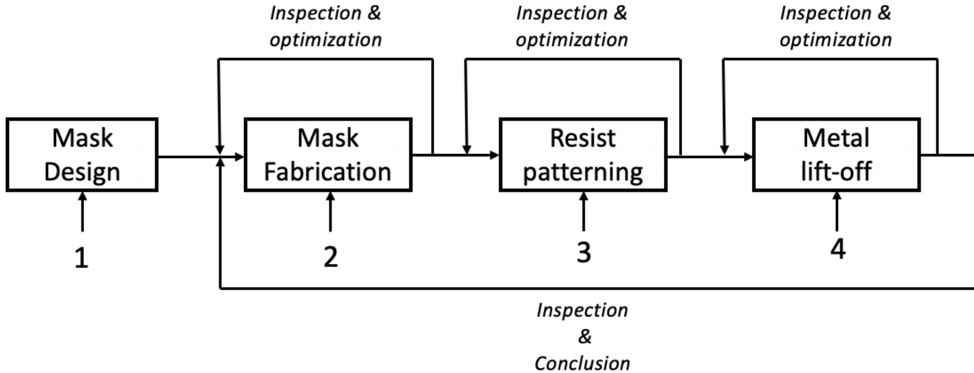

Figure 10: Block diagramm of the project developpment

1. Implementation of the new layout with appropriate feature for lift-off profile inspection.
2. Optimization of the VPG200 parameters in order to achieve critical dimension on the mask
3. Optimization of ASML Stepper parameters in order to achieve critical dimension on wafers
4. Optimization of deposition techniques and parameters

Note that an inspection is made between each step in order to interpret the optimisation parameters set during particular steps. Those inspection are first made by optical microscopy and further continue with SEM pictures for accurate measurements. The step by step inspection is necessary in order to independently optimise the entire process and limit correlation between parameters at different levels of the project.

3.2 Mask design and fabrication

Two Mask designs were defined using KLayout software in order to investigate two main points:

- Mask for optimization of the reticle fabrication parameters
- Reticle for optimization of the DUV stepper parameters

The typical process flow of mask fabrication is shown in Figure 13 and can be found in annexe A. The writing of the mask is made using the Heidelberg Instruments VPG200 - Photoresist Laser Writer and the Hamatech HMR900 for the development, both equipments are available in the CMi. This step is particularly important as we are approaching the critical dimension possible with this equipment. The first step is to chose the size of the write head between 20, 10 and 4 mm. This will set the critical dimension achievable. Note that there is a trade-off betweeen the critical dimension and the throughput as it is positively correlated with the size of the head. The choice of the head set the illumination factor. Two other parameters are then useful for optimisation: the Pneumatic Defocus (DF) which is set to zero at the top of the resist and shift positively downward inside the resist and the laser intensity in percentage of maximum available power which controls the exposure dose. The main fixed settings used are resumed in table 1.

Write Head	Illumination Factor	Beam Diam.	CD	Pixel
4 [mm]	215 [$\frac{mJ}{cm^2}$]	0.6 [μm]	0.7 [μm]	1000

Table 1: Fixed VPG200 parameters [11]

Two main patterns were implemented for this project and are presented in figure 4. (a) is the so-called "damier" pattern which is used for assessment of the lift-off of parallel line and its profil, as well as the limit between staggered fingers. In this example, the damier is made of three line of four fingers with a define width and pitch, which is always equal to two time the width. Several designs with different combinations of those parameters will be made. (b) represents a 5 fingers IDT electrode that was added to the design as a proof of concept to assess their feasibility. Different combinations of the three parameters of the electrode will also be made.

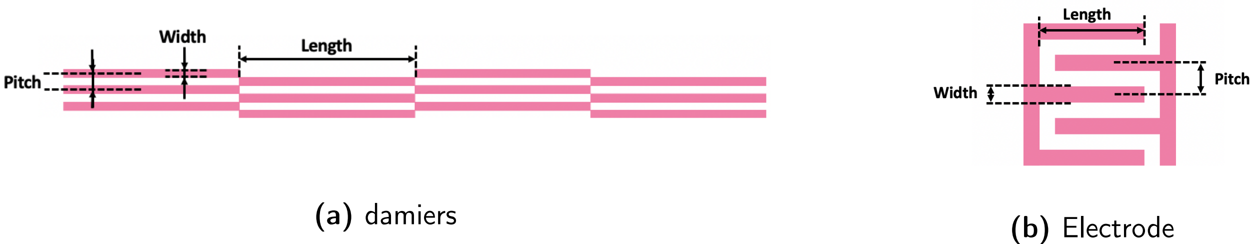

(a) damiers

(b) Electrode

Figure 11: CAD layout of the two main implemented patterns

3.2.1 Pattern for reticle parameters optimization

The pattern for the reticle parameters optimization is a pattern that will be written in a regular Cr Blank Mask. It allows the SEM inspection of the Mask which is not possible on the reticle due to non-compatibility of the process with the non-contamination requirements of the stepper. This pattern is slightly different than the one that will be printed on the reticle due to the fact that we wanted to decrease its overall size in order to check as many dose parameters as possible when writing the Mask. In Figure 12, the upper part represents the pattern in the optimized direction for writing with the VPG, as the head is going in the vertical direction. 1. represents an array of electrodes with the pitch varying in the horizontal direction and a critical dimension of 600 [nm]. In the vertical dimension, the number of fingers of each electrodes is changed. 2. represents an array of "damier", the critical dimension is set to 600 [nm] for the pitch and width of the first one. The value for both paramters is then increase in the vertical

dimension. 3. illustrates the different CD bias added to the pattern to check if it could have a positive impact on the final dimension. The two other patterns of the upper parts are negatives of the already mention features to have the possibility to compare with an etching process of the metal. The lower part represents the same pattern than the upper part with a 90 degree change in the writing direction relatively to the patterns.

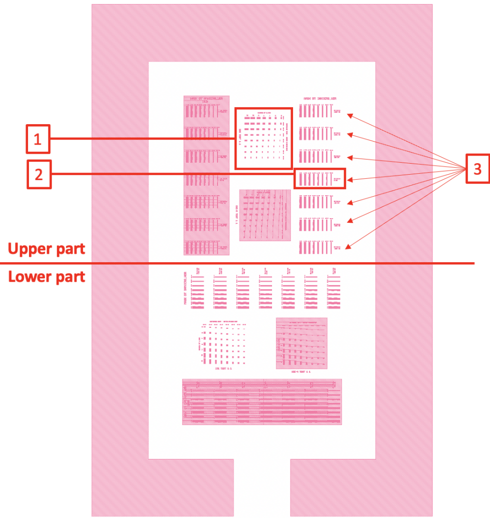

Figure 12: Mask layout for reticle optimization

3.2.2 Pattern for assessment of the lift-off and profile

The pattern for assessment of the lift-off is the one that is printed on the reticle. The doses used are defined following the optimization of the previously mention step. The final pattern is illustrated in Figure 13. Part 1. is the implementation of the "damier". The array is made the same way than explained above with the difference that a very long finger is added in the middle of the damier to allow cleaving of the chip for inspection of the profile. 5. represents the different CD Bias also implemented. 2. is an array of 22 electrodes. 3. is an array of 22 negative electrodes. 4. is the "damier" pattern in the opposite writing direction. Finally, 6. represents 20 [μm] structure used to inspect the success of the lift-off. Note that the dimensions written on the reticle are the wafer level dimensions - four time smaller than the reticle dimensions - due to the reduction lens used in the stepper.

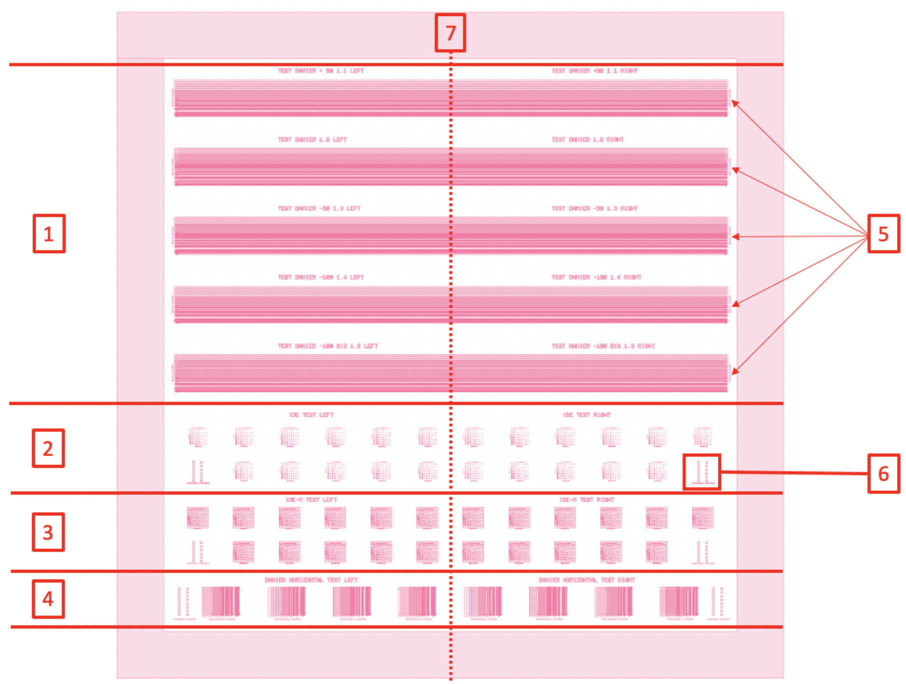

Figure 13: CAD layout of the final reticle chip

3.3 Process Flows

In this section, we will discuss the process flows elaborated and the different steps that lead to the manufacture of the devices. The basic steps consist in the deposition of a platinum thin film on top of a silicium wafer with the help of a lift-off process. A bottom up approach was performed using a DUV positive photoresist and a chromium reticle for DUV stepper lithography. An alternative process flow with a top down approach and the etching of the metal will also be discussed, it was use as a comparison between the differents methods and the final achievable critical dimensions.

Reticle fabrication

The reticle fabrication step and parameters are explained in section 3.2.

Photoresist coating, exposure and development

The frist step consists in the choice of the wafer. Here we use Silicium prime wafer TTV2 available in the CMi. Concerning the choice of the photoresist, only two are available in the CMi for DUV lithography. We used both of them to compare their performances for our application. Note that a thicker resist is more suitable for lift-off but a thinner resist allows for better resolution of the patterned resist after development. The values are resumed in table 2.

Resist name	Thickness	Coating recipe	Development recipe
M108Y	450 [nm]	2014 [μm]	2100
M35G	1.2 [μm]	2024 [μm]	2101

Table 2: Photoresist coating and development parameters

The coating and the development of the photoresist is made using the Süss ACS200 GEN3

equipment in CMi zone 1, the final process step is illustrated in Figure 14. Note that in every case, a HMDS priming is done prior spin-coating in order to insure a proper adhesion of the potoresist on the wafer. This step is included in the ACS recipe. The exposure is done using the ASMl PAS 5500/350 C - DUV stepper equipment in CMi zone 5. The two main exposure parameters for the DUV stepper are the dose and the focus. They both will be experimentally optimised starting with the theoretical value found on the CMi website and previous experience from the operators. Finally, a post exposure bake (PEB) was made to stabilize the resist before developemnt. As already mention, this step is particularly critical and needs to be done immediately after exposition.

Figure 14: Photoresist exposure and development schematic

Surface activation and thin film metal deposition

Two deposition principles were used for the metal deposition, sputtering using the Pfeiffer Spider 600 or electron beam evaporation with the EVA 760 in CMi zone 11. In term of quality of deposition, sputtering has several advantages. The main ones being a better adhesion, coverage and uniformity of the metal deposited compare to the evaporation process. However, this process is slower, more complex, more expensive and uniformity needs to be avoided in order to optimise the success of lift-off, thus the EVA 760 was preferred. Note that a better option to decrease uniformity would have been to use the LAB 600 H equipment, as the crucible is placed further away from the wafer than in the EVA 760.

As mentioned before, an important parameter in the manufacture of our device is the adhesion between the silicon and the thin metal film. To optimise this adhesion, we did a surface cleaning using high frequency plasma with the TEPLA 300 in CMi zone 11 to strip the possible remaining photoresist and activate the surface. The parameters used were 200 W for 30 seconds with the wafer place horizontally for a better consistency of the process. Added to that, a 10 [nm] titanium buffer adhesion layer was also deposited prior to the 40 [nm] platinum layer.

Figure 15: Surface activation and thin film metal deposition schematic

Lift-off of the photoresist

The next process consists in the lift-off of the remaining photoresist in order to keep only the deposited device pattern on the silicium wafer, this is done using the photolithography wet bench in CMi zone 1. The wafer is placed inside a ultrasonic bath containing remover-1165 for 5 minutes and is then placed inside an beaker for static lift-off. The total duration of the lift-off process are experimentally optimised.

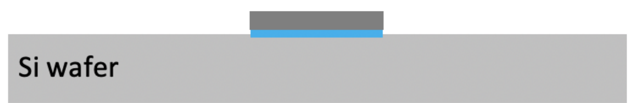

Figure 16: Lift-off of the photoresist schematic

SEM examination

In order to inspect the wafer, SEM examination was performed using Zeiss LEO 1550 in CMi zone 1. This step was implemented for the Chromium Mask and the final devices after lift-off. Unfortunately, the inspection of the photoresist prior evaporation mentionned in Figure 10 was skipped due to time restriction and considering the complexity of this step as the resist is a non-conducting material which prevent us from having good image quality with the SEM.

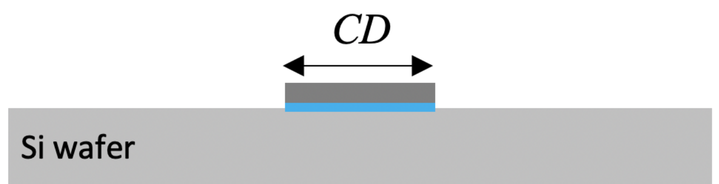

Figure 17: SEM Examination schematic

Alternative process flow

Finally, we implemented a different process flow defined in annexe B. In this case, the metal was deposited before the photoresist patterning using the EVA 760 and the same parameters as previously mentionned. The photoresist coating, exposition and development is used to define the pattern on top of the metal. The metal will then be etch by reactive ion etching using the STS Multiplex ICP plasma etcher in CMi zone 2. In addition, we used a 65 [nm] BARC layer on one of our wafer that we needed to remove before etching of the metal, for that we used the SPTS APS: dielectric plasma etcher in CMi zone 2.

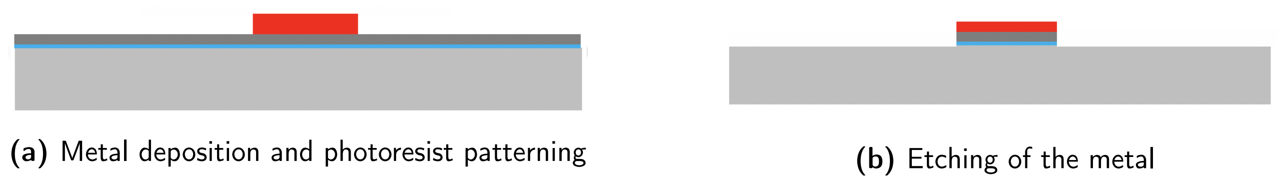

(a) Metal deposition and photoresist patterning

(b) Etching of the metal

Figure 18: Alternative process flow schematic

Note that after etching of the metal, the resulting photoresist that is not completely gone is remove using the TEPLA plasma stripper. Also, the remaining pattern are inverted and we will thus inspect the negative tone electrode illustrated in paragraph 3.2.2.

4 Results and discussions

4.1 Mask for reticle optimization

In this section we are presenting the results of the reticle optimisation values. As previously mentionned, the two main important parameters to tune on the VPG are the dose intensity and the defocus. In our case and following advices from the CMi staff, we only tuned the intensity in order to define the dose with the better matching between the size of the gap, which represents the printed area and its theoretical value for the critical dimension feature. We printed a vector of the pattern presented in Figure 12 with a fixed value of -30 for the defocus and the intensity dose varying from 8.5 [%] to 17.5 [%] with step of 0.5 [%] each.

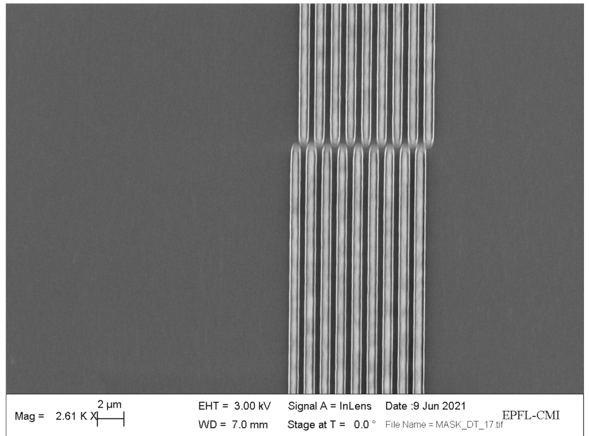

(a) SEM image of damier for 9.5 [%] dose intensity

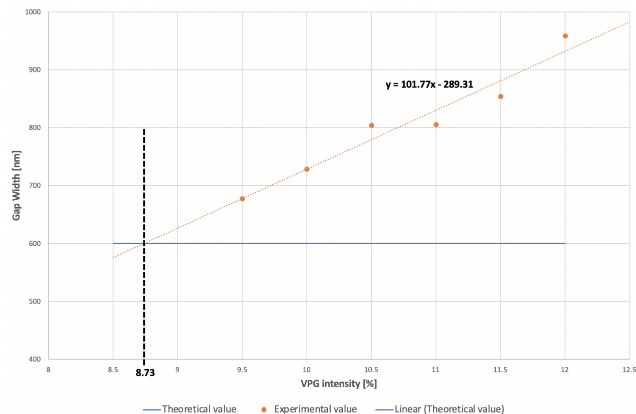

(b) Theoretical and experimental value of the gap width over VPG intensity

Figure 19: Optimization results of the reticle fabrication using VPG200

Figure 19 (a) represents the printed pattern on the Mask. Here, the darker area represents the chrome and the lighter area the written part of our pattern. First, we can see that the isotropic etching chemistery used for the mask processing steps had an impact on the crossing between two lines. This is a parameter we can't control but that we have to take into account when defining the most accurate dose. We measured the gap for various value of intensity in order to define a trendline. In Figure 19 (b), the blue line represents the 600 [nm] targeted value and the orange dots the measured value of the gap. We can observe that there is a linear relation between the intensity of the dose and the error in gap width. We theoretically calculated the optimised intensity by matching the trendline equation to the pattern value of 600 [nm] and found an theoretical optimal intensity of 8.73 [%].

4.2 Final reticle fabrication

Based on the theoretical value found in section 4.1, we defined a new 9 times 9 matrix with the same chip pattern but with different dose of intensity for the reticle as illustrated in Figure 20, where the intensity dose in [%] is illustrated in the middle of each chip.

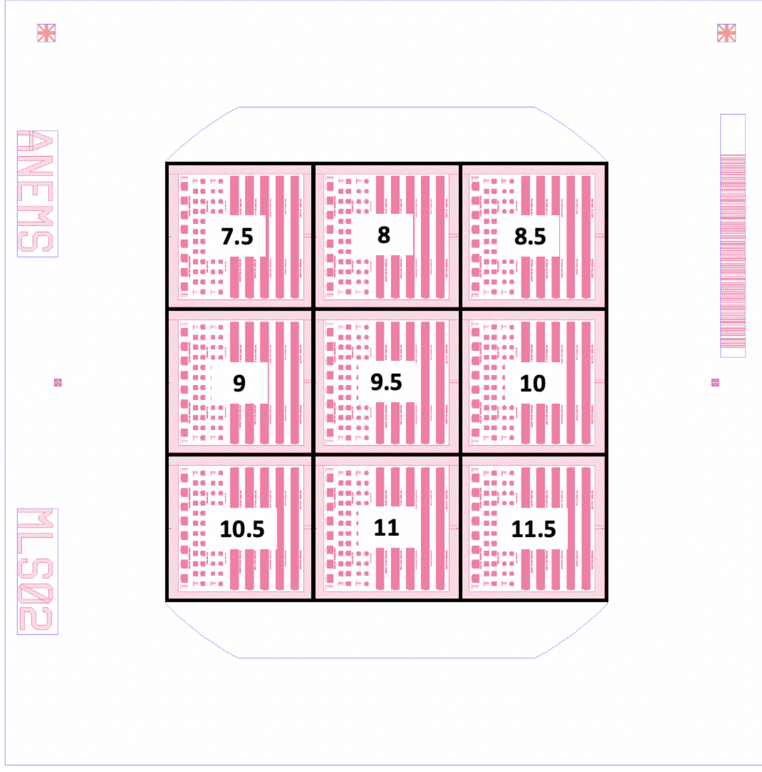

Figure 20: Final reticle intensity dose mapping

Having multiple dose represented will help us assess the better combination of successive expositions from the VPG and stepper for a successful final patterning of the resist which should be :

- VPG underexposition & Stepper overexposition
- VPG overexposition & Stepper underexposition
- VPG & Stepper individually optimised exposition

The value of the VPG parameters used for the reticle fabrication are resumed in table 3.

Intensity [%]	Defocus [mm]	Head size [mm]	Pixel
7.5-11.5	-30	4	1000

Table 3: VPG paramters for the final reticle

4.3 Results of wafer processing

In this section, the different results on each wafer will be presented. The summary of each process made for each wafer is shown in table 4. The lift-off process is define as the default process presented is section 3.3 and can by found in annexe A. The Etching process is define as the alternative process flow in the same section and can be found in annexe B).

	Wafer ID	Wafer type	Reticle	Photoresist	Process
1	CMi 01 05 86 03	Si TTV2	ANEMS S01	M108Y	Lift-off - EVA
2	CMi 01 05 85 99	Si TTV2	ANEMS S01	M35G	Lift-off - EVA
3	CMi 01 05 85 97	Si TTV2	ANEMS S02	M35G	Lift-off - EVA
4	CMi 01 05 86 05	Si TTV2	ANEMS S02	M35G	Lift-off - SPUTTER
5	CMi 01 05 86 00	Si3N4 TTV2	ANEMS S02	M108Y	Etching
6	CMi 01 05 83 55	Si3N4 TTV2	ANEMS S02	M108Y + B	Etching

Table 4: Wafers processing results resume

4.3.1 First Batch: Wafer 1 & 2

The two first wafers were made using the previously written reticle made by R. Douat and the already existing job made during the previous semester project for stepper exposition. The goal was to have a first try on the lift-off process and evaluate the difference between the two resists. As expected, the results were that the lift-off was not succesfull with the thinner M108Y resist. Some resist residual could be observed even after multiple ultrasound bath. Concerning the second wafer, the lift off was performed and the critical dimension observed was 300 [nm] for "damier" pattern and 350 [nm] for the electrode pattern as shown in Figure 21.

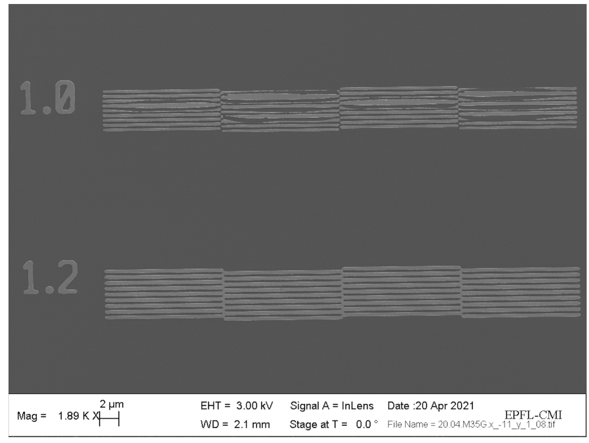

(a) Damier feature of 300 [nm]

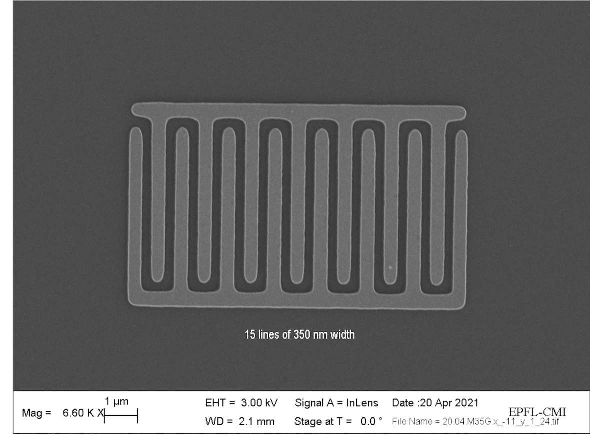

(b) Electrodes feature of 350 [nm]

Figure 21: SEM pictures of damier and electrodes for wafer 2

In (a), the dimension is the reticle level dimension in [μm]. The value of the parameters are resumed in table 5. We can see in the picture and from the interpretation of the MTT value that there is an overexposition. As the reticle itself was overexposed, a lower value of the VPG intensity dose could lead to a better accuracy in the linewidth.

VPG [Intensity ; Defocus]	Stepper [Intensity ; Focus]	Feature type	PT Linewidth MTT [nm]
[20.5 ; -37]	[37 ; 0]	Damiers 300 nm	+99.7
[20.5 ; -37]	[37 ; 0]	Electrode 350 nm	+56.1

Table 5: Wafer 2 measurement results resume

4.3.2 Second Batch: Wafer 3 & 4

The two next wafers were made using the new reticle presented in section 4.2 and M35G photoresist following results conclusion from the first batch. Concerning the stepper exposition parameters, the focus was fixed following CMi operator advices and in order to have only one unknown parameter to define the best dose. The minimum and maximum dose were defined to be centered around the value previously found during the first batch. We used a meander disposition to exposed the full reticle with different dose on the wafer as shown in Figure 22

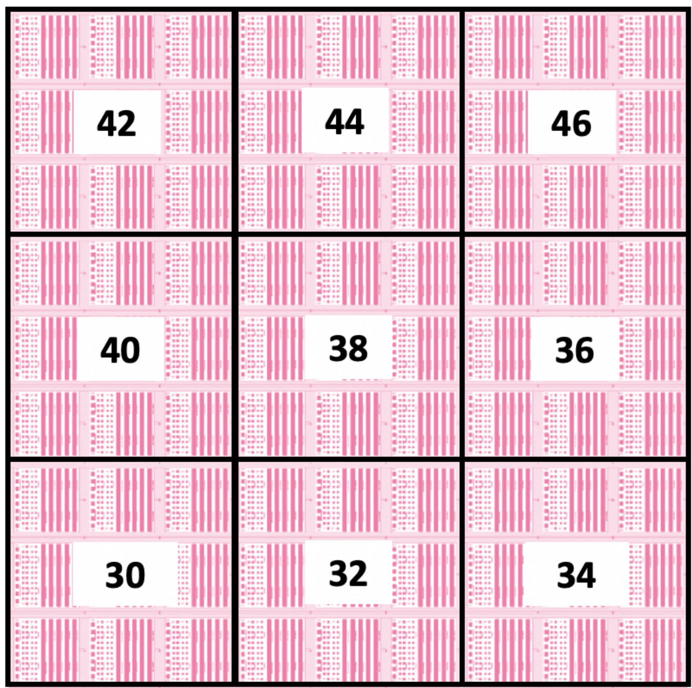

Figure 22: Final wafer intensity dose mapping

Each black square represents the exposed reticle with its particular dose in $[\frac{mJ}{cm^2}]$. Each square is 217.5 [mm] large and is spaced with the next square from 1 [mm]. The value of the focus for the whole exposition is -0.2 [μm].

The main difference between those wafer 3 and 4 is the metal deposition method. As expected, the results were that the lift-off was less succesfull with the sputtered metal, our hypothese is that the more important uniformity of the sputter deposition decrease the lift-off success rate. Some resist residual could be observed even after multiple ultrasound bath as we can see in Figure 23.

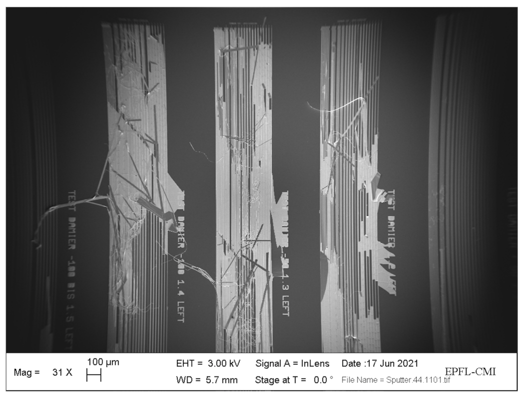

Figure 23: Remaining resist during liftoff for wafer 4

We will thus focus on wafer 3 for the results of the lift-off and more precise measurements. The first inspection was a mapping of the smallest critical dimension take could be observed for the couple VPG dose - Stepper dose, the feature that is observed in this case is the long damier with no CD Bias for the 81 different combination. The results of this observation is illustrate in Figure 24.

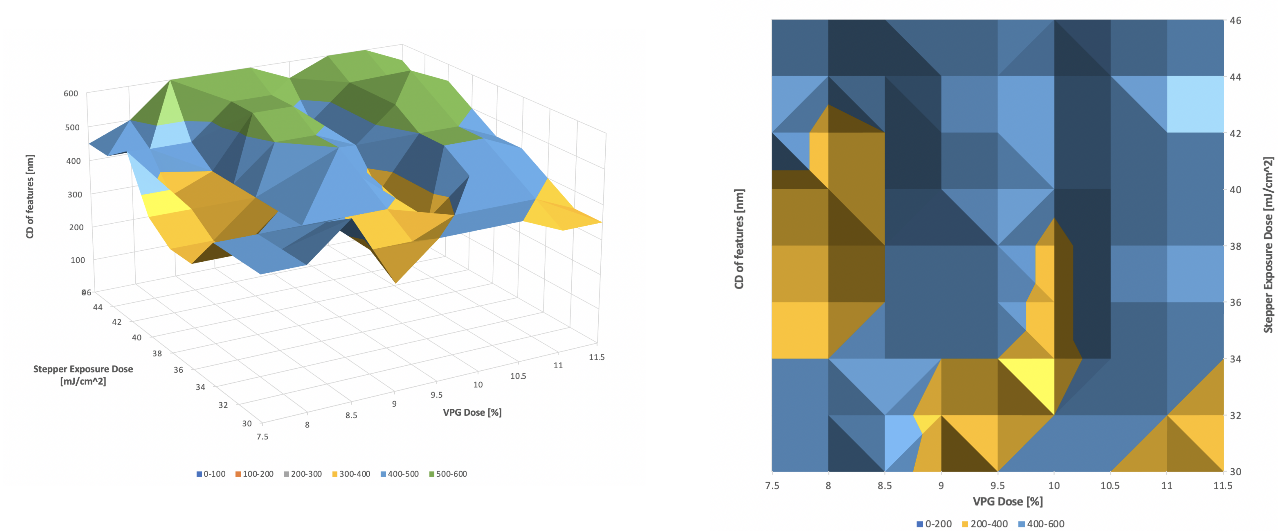

Figure 24: Critical Dimension inspection of damier feature for wafer 3

We can see that the smallest feature that could be recovered after the lift-off is 300 [nm] and that there is two main VPG dose value that brought interesting results which are 8 [%] and 10 [%] of intensity. We can also conclude that there is a dependance between the VPG and the stepper exposition that needs to be experimentally optimised. An overexposition with the VPG can be overturned by an underexposition with the stepper and vice-versa. However, we can see that when the exposition is high in both cases, the smallest observable feature has a bigger dimension. Thoses graphs also raise the hypotheses that the lift-off success is more dependant on the VPG dose optimisation that on the stepper dose based on the two yellow vertical spot observation.

Another interesting observation is that there is a difference in the broken structure of under-exposed and overexposed chip. In Figure 25, We can see that on the left, there is no remaining metal for smaller structure than the critical dimension observed but on the right, the broken structures are made of a single platinum area. It is difficult to know if this is due to the resist patterning prior deposition as we didn't inspect them but we are making the hypothese that independently from the VPG and Stepper dose optimisation, there might be a resolution limit

for pattern due to the lift-off process itself. Our hypothese is also strenghenth by the previsouly made observation on wafer 1 and 2, where we knew that the reticle was overexposed but the critical dimension of pattern observd with the best combination of paramters was also equal to 300 [nm].

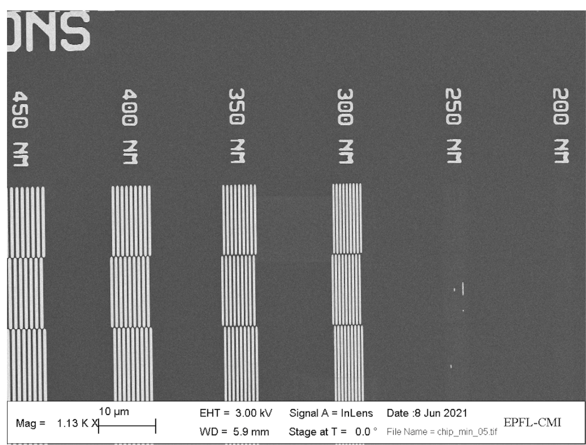

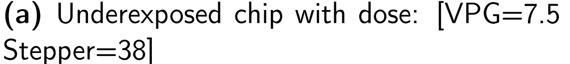
(a) Underexposed chip with dose: [VPG=7.5 ; Stepper=38]

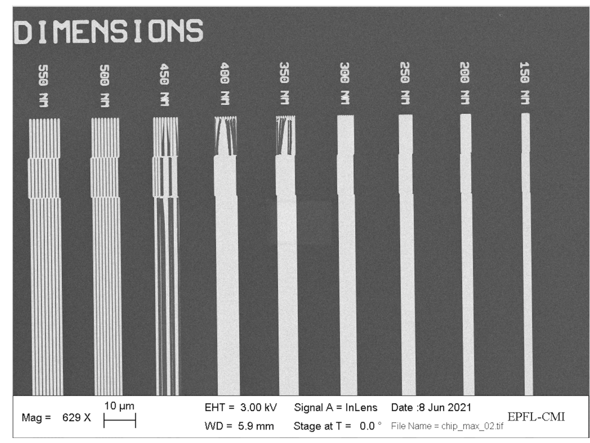

(b) Overexposed chip with dose: [VPG=11.5 ; Stepper=44]

Figure 25: Over and underexposed chips comparison for wafer 3

The main types of measurements made on the devices were the linewidth and gapwidth in nanomètre using SEM image processing tool. Those measurements were principally made on damier structures with various size and exposition parameters. Figure 26 (a) shows the experimental linewidth (orange) and gapwidth (grey) of 500 [nm] damiers structure over the whole VPG intensity spectrum for a fixed value of 38 $\frac{mJ}{cm^2}$ of the stepper dose. In Comparison, Figure 26 (b) shows the experimental linewidth (orange) and gapwidth (grey) of 400 [nm] damiers structure over the whole spectrum of stepper exposure dose for a fixed value of 8 [%] for the VPG intensity. It is interesting to note that we have a linear relation for both the VPG dose and the Stepper exposure dose with the value of the MTT for the measured features. Thoses graphs can be used for optimization of accuracy of the final structure and we can see that already in the case of (b) we can achieve a precise similar dimension between theoretical and experimental values. However, those linear relations are intimately linked to the critical dimension and pattern of the features and need to be optimised in each case. For our observation, the optimal couple [VPG intensity ; Stepper dose] for a 400 [nm] damier strucures is equal to [8 ; 30.5].

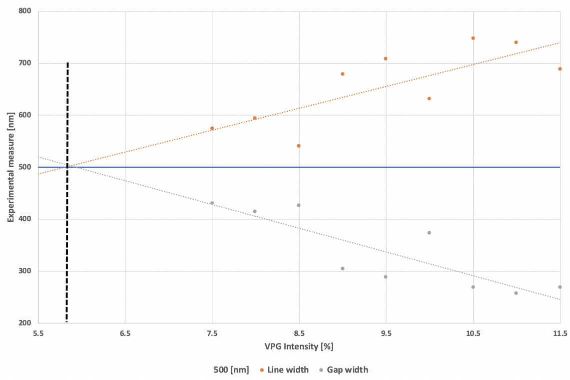

(a) 500 [nm] damiers structure for differents VPG intensity

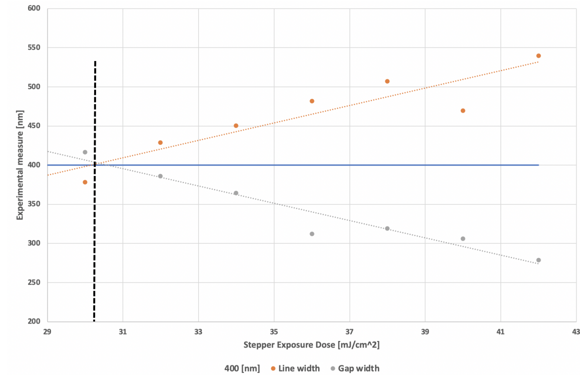

(b) 400 [nm] damiers structure for differents Stepper exposure dose

Figure 26: VPG and stepper exposition parameters results for wafer 3

Note that the exposition parameters also have an impact on the reproduction of the pattern at the intersection of fingers in the damier structure. The line between fingers is in most of the case continuous for an overexposition and increase similary with the designed pattern when we come closer to the optimised exposition parameters.

Figure 27 shows the impact of CD bias on the reticle for (a) 400 [nm] and (b) 300 [nm] damier structure. Note that here the value of the CD bias is on the reticle level. The actual change for a -100 [nm] CD Bias on the wafer level would thus be -25 [nm]. Thoses graphs show a linear dependance between the value of the CD Bias and the experimental measured linewidth that could also be used for optimization of the manufactured devices. Note that in the case of the 400 [nm] damier, the slope represents well the change in CD bias: 200 [nm] change of CD Bias leads to 50 [nm] reduction in the metal linewidth. However, as we decrease the dimension, this relation becomes less precise as illustrated by the results obtained in (b). It shows once again the difficulty to work close to the critical dimension of reticle fabrication equipment.

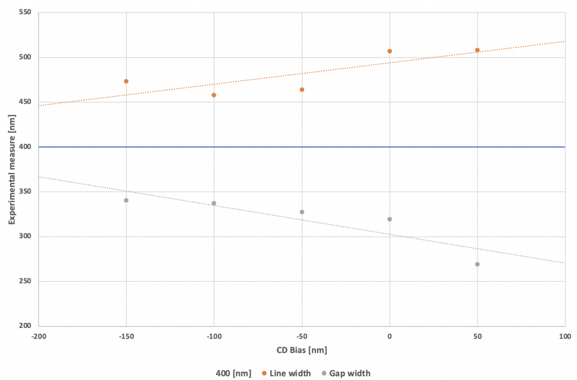

(a) 400 [nm] damiers structure with different CD Bias, a VPG dose of 8 [%] and a stepper exposure dose of 38 $\frac{mJ}{cm^2}$

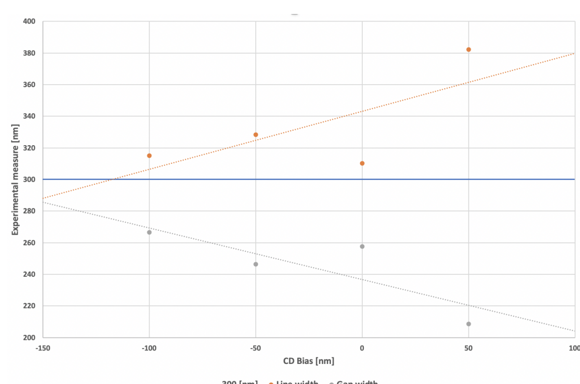

(b) 300 [nm] damiers structure with different CD Bias, a VPG dose of 8 [%] and a stepper exposure dose of 38 $\frac{mJ}{cm^2}$

Figure 27: CD Bias parameters results for wafer 3

The two best features observed are presented for the lift-off process of wafer 3 in Figure 28. In both pictures, the deposited platinum is in light grey. On the left we can observed the damier pattern with a measured linewidth of 310.1 [nm]. On the right, we can see a 15 fingers electrode with a measured linewidth of 432.6 [nm]. This represents the best achived lift-off for our two main patterns and act as a proof of concept that the lift-off process can be used for

considerably reduced dimension and using DUV lithography for resist patterning. The main measurements made on those two features are resumed in table 6.

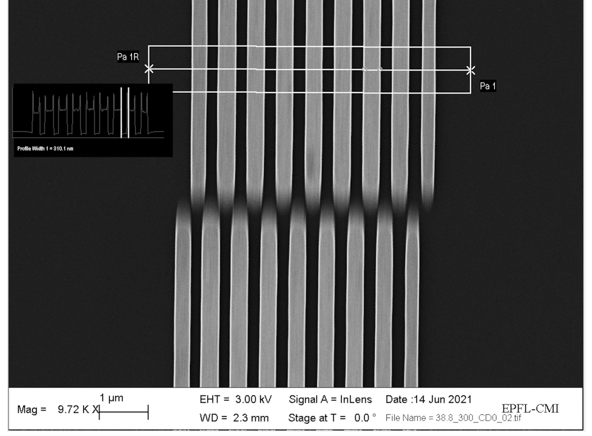

(a) 300 [nm] Damiers pattern lift-off

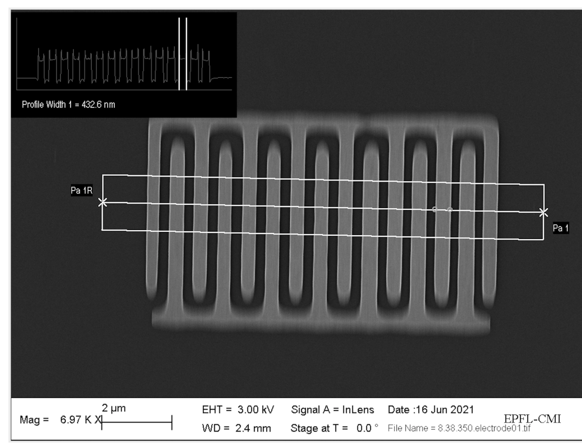

(b) 350 [nm] Electrodes pattern lift-off

Figure 28: SEM pictures of the smallest achievable damier and electrode feature for wafer 3

VPG Dose	Stepper Dose	Theoretical linewidth [nm]	Experimental linewidth [nm]	Experimental gapwidth [nm]	Type of feature	CD Bias
8	38	300	310.1	257.7	Damiers	0
8	38	350	432.6	240.4	Electrodes 15	0

Table 6: Resume of measurements made on the smallest achievable damier and electrode feature for wafer 3

Finally, one of the goal of the new design was to enable the inspection of the profile of the lift-off after cleaving of the wafer as explained in section 3.2.2. This step was investigate and a cleaving of the third wafer was made. However, we couldn't achieve a satisfying SEM inspection of the cleaved wafer as shown in Figure 29. We can see that some metal was deposited represented by the bright discontinuous line in the middle which should be the profile of a 350 [nm] damier with VPG intensity parameter equal to 8 [%] and the stepper dose equal to 38 $[\frac{mJ}{cm^2}]$. Unfortunately, the SEM equipment didn't allow us to inspect more precisely the features and have a more compelling view of the lift-off profile.

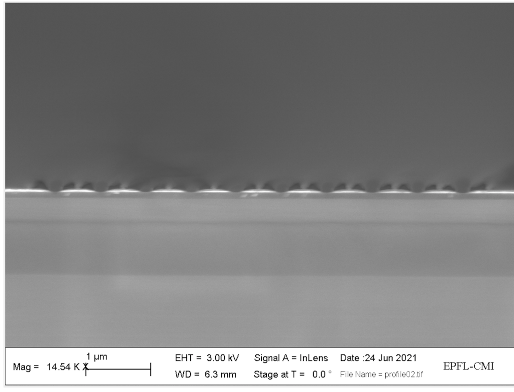

Figure 29: SEM picture of the profile of a damier structure after cleaving for wafer 3

4.3.3 Third Batch: Wafer 5 & 6

Following the purpose of comparing the different possibilities of manufacture for thoses patterns, we used another process where we deposited the thin metal film prior patterning of the resist. An etching of the metal was then done after resist coating, exposure and development. In this case, two wafers were processed using M108Y resist, as it enable better pattern resolution of the resist and we do not need high walls profile like in a lift-off process. The stepper exposition was made with the same meander than for the M35G (see Figure 22) resist only changing the minimum dose to 12 $[\frac{mJ}{cm^2}]$ and keeping the same steps. In addition, wafer 6 was process using the new clean-track available with the CMi DUV stepper which was still under optimization and also adding a BARC layer. In both wafers, we observed the negative patterned electrodes to have the same final results as in the liftoff process as we changed from a bottom-up to top-down approach with impact the needed tone of the reticle. The best observed feature in wafer 5 in presented in Figure 30 and represents a 15 fingers electrode pattern of 350 [nm], which is similar to what we have observed with the lift-off process. In another hand, for wafer 6, the smallest observed feature is a 15 fingers electrode pattern of 150 [nm], eventhough we can observed some short circuits between the two sides of the electrodes. This represents a huge improvement in the resolution of the smallest achievable pattern and comes very close to our inital objective of having a 150 [nm] resolution. This process gives us also a good information about the efficienty of using a BARC layer in the process and we believe that the direct processing of the wafer by the clean track was a big improvements too.

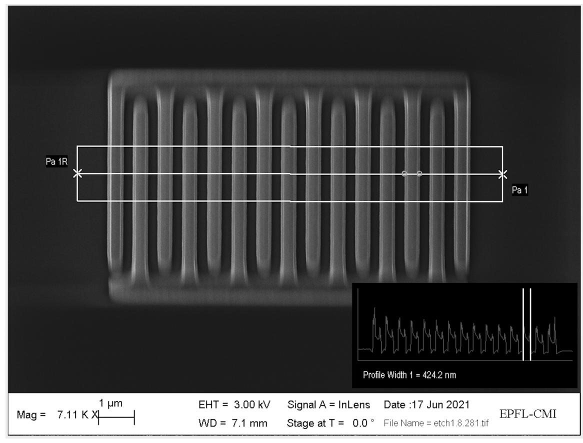

(a) Wafer 5 best observed electrode feature

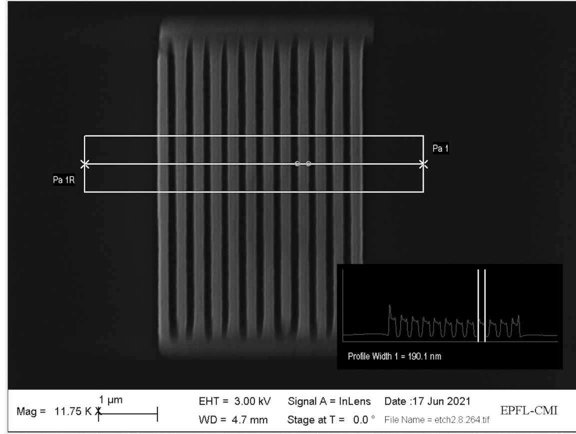

(b) Wafer 6 best observed electrode feature

Figure 30: SEM pictures of the smallest achievable electrode feature for wafer 5 and 6

Table 7 resume the main measurements made on the electrodes presented in Figure 30 with respectively the first line referring to (a) and the second line referring to (b). It shows that a 190.1 [nm] thick line was observed on wafer 6, which repesents the feature with the better resolution of the whole project.

VPG Dose	Stepper Dose	Theoretical linewidth [nm]	Experimental linewidth [nm]	Experimental gapwidth [nm]	Type of feature	CD Bias
8	28	350	424.2	267.1	Electrode 15	0
8	28	150	190.1	133.1	Electrodes 15	0

Table 7: Resume of measurements made on the smallest achievable electrode feature for wafer 5 and 6

5 Conclusion

Within the scope of this project, we have assessed the feasibility of a new manufacturing method for scaling down contour mode resonators (CMRs) used as oscillators in RF front-ends. The possibility to tune the operating frequency by design would allow us to match the requirements of the new 5-G telecommunication industry.

The fabrication of the device was made using DUV stepper technology available in the CMi enabling us to increase the resolution to 150 [nm]. In the first part, a meticulous state-of-the-art literature review was made to define the best process that could be implemented in the CMi but also to found alternative solutions that could be further implemented to optimize the fabrication of the interdigitated fingers array needed in CMRs.

Two main fabrication steps were then optimized in the CMi which are the optimization of the reticle used for patterning the IDT and the exposition parameters used in the DUV stepper. The main process flow was to use a lift-off process for the metal deposition but an alternative etching process flow was also investigated to compare the final achievable dimension of the design. A damier feature and electrode were printed on a silicon wafer and we found that the critical achievable dimension after optimization of the parameters for a lift-off process was a linewidth of 300 [nm] for damier structure and 350 [nm] for electrode structure with respectively an MTT of 10.1 [nm] and 82.6 [nm]. We found that the pair of exposition parameters [VPG; Stepper] had a considerable impact on the success of the lift-off and needs to be optimized independently.

However, it was difficult to assess if the resolution could be even better by optimizing the exposition parameters or if the resolution limit is mainly due to the lift-off process complexity at such a small dimension. On the other hand, we investigate other process flows where the lift-off was replaced by etching of the metal and found very promising results enable by the possibility of using a BARC layer in this process. The final achievable feature dimension was an electrode array of 150 [nm] linewidth with an MTT of 40.1 [nm].

Further research steps could be implemented to optimize even more the critical dimension.In this scope, an assessment of the resist pattern before metal deposition could be very interesting, as well as an investigation on additional lift-off processes that are discussed in the literature review.

Finally, one of the goals of this project was to investigate the metal profile after lift-off but we were unable to achieve it with cleaving and SEM examination. Thus, finding a new solution for the assessment of the profile would also represent a great follow-up to this project.

References

[1] Andrea Lozzi et al. "Evidence of Smaller 1/F Noise in AlScN-Based Oscillators Compared to AlN-Based Oscillators". In: *Journal of Microelectromechanical Systems* 29.3 (2020), pp. 306–312. DOI: 10.1109/JMEMS.2020.2988354.

[2] Muhammad Faizan and Luis Guillermo Villanueva. "Frequency-scalable fabrication process flow for lithium niobate based Lamb wave resonators". en. In: *Journal of Micromechanics and Microengineering* 30.1 (Dec. 2019). Publisher: IOP Publishing, p. 015008. ISSN: 0960-1317. DOI: 10.1088/1361-6439/ab5b7b. URL: https://doi.org/10.1088/1361-6439/ab5b7b (visited on 06/19/2021).

[3] Andrea Lozzi et al. "Al0.83Sc0.17N Contour-Mode Resonators With Electromechanical Coupling in Excess of 4.5%". In: *IEEE Transactions on Ultrasonics, Ferroelectrics, and Frequency Control* 66.1 (2019), pp. 146–153. DOI: 10.1109/TUFFC.2018.2882073.

[4] Gianluca Piazza. "Contour-Mode Aluminum Nitride Piezoelectric MEMS Resonators and Filters". en. In: *MEMS-based Circuits and Systems for Wireless Communication*. Ed. by Christian C Enz and Andreas Kaiser. Integrated Circuits and Systems. Boston, MA: Springer US, 2013, pp. 29–54. ISBN: 978-1-4419-8798-3. DOI: 10.1007/978-1-4419-8798-3_2. URL: https://doi.org/10.1007/978-1-4419-8798-3_2 (visited on 06/19/2021).

[5] Andrea Lozzi. *AlN and AlScN contour mode resonators for MEMS-based RF front ends*. fr. Number: THESIS Publisher: EPFL. 2019. DOI: 10.5075/epfl-thesis-7247. URL: https://infoscience.epfl.ch/record/268269 (visited on 06/20/2021).

[6] Garry J. Bordonaro. "DUV Photolithography and Materials". In: *Encyclopedia of Nanotechnology*. Ed. by Bharat Bhushan. Dordrecht: Springer Netherlands, 2012, pp. 590–604. ISBN: 978-90-481-9751-4. DOI: 10.1007/978-90-481-9751-4_370. URL: https://doi.org/10.1007/978-90-481-9751-4_370.

[7] Rajesh Menon et al. "Maskless lithography". In: *Materials Today* 8.2 (2005), pp. 26–33. ISSN: 1369-7021. DOI: https://doi.org/10.1016/S1369-7021(05)00699-1. URL: https://www.sciencedirect.com/science/article/pii/S1369702105006991.

[8] E. Reichmanis and L.F. Thompson. "Chemistry and processes for deep-UV resists". In: *Microelectronic Engineering* 13.1 (Mar. 1, 1991), pp. 3–10. ISSN: 0167-9317. DOI: 10.1016/0167-9317(91)90037-E. URL: https://www.sciencedirect.com/science/article/pii/016793179190037E.

[9] C. W. Wilkins et al. "Deep UV photolithographic systems and processes". In: *Polymer Engineering and Science* 23.18 (Dec. 1983), pp. 1025–1028. ISSN: 0032-3888, 1548-2634. DOI: 10.1002/pen.760231810. URL: http://doi.wiley.com/10.1002/pen.760231810 (visited on 06/17/2021).

[10] Nobuo TAKAHASHI and Hiroki Kikuchi. "Rayleigh Criterion: The Paradigm of Photolithography Equipment". In: *Annals of Business Administrative Science* 16 (July 13, 2017). DOI: 10.7880/abas.0170525a.

[11] *CMi – Center of MicroNanotechnology*. URL: https://www.epfl.ch/research/facilities/cmi/ (visited on 06/19/2021).

[12] *Patterning the World: The Rise of Chemically Amplified Photoresists*. Science History Institute. Oct. 2, 2007. URL: https://www.sciencehistory.org/distillations/patterning-the-world-the-rise-of-chemically-amplified-photoresists (visited on 06/19/2021).

[13] *C.L. Henderson Group - Introduction to Chemically Amplified Photoresists.* URL: https://sites.google.com/site/hendersonresearchgroup/helpful-primers-introductions/introduction-to-chemically-amplified-photoresists (visited on 06/19/2021).

[14] Hiroshi Ito. "Chemically amplified resists: past, present, and future". In: *Advances in Resist Technology and Processing XVI.* Advances in Resist Technology and Processing XVI. Vol. 3678. International Society for Optics and Photonics, June 11, 1999, pp. 2–12. DOI: 10.1117/12.350143. URL: https://www.spiedigitallibrary.org/conference-proceedings-of-spie/3678/0000/Chemically-amplified-resists-past-present-and-future/10.1117/12.350143.short (visited on 06/19/2021).

[15] Theodore Manouras and Panagiotis Argitis. "High Sensitivity Resists for EUV Lithography: A Review of Material Design Strategies and Performance Results". In: *Nanomaterials* 10.8 (Aug. 14, 2020). ISSN: 2079-4991. DOI: 10.3390/nano10081593. URL: https://www.ncbi.nlm.nih.gov/pmc/articles/PMC7466712/ (visited on 06/19/2021).

[16] Tim Brunner. "Optimization of optical properties of resist processes". In: *Proceedings of SPIE - The International Society for Optical Engineering* 1466 (June 1, 1991). DOI: 10.1117/12.46410.

[17] Wen-Bing Kang et al. "Bottom Anti-Reflective Coatings for DUV Lithography". In: *Journal of Photopolymer Science and Technology - J PHOTOPOLYM SCI TECHNOL* 10 (Jan. 1, 1997), pp. 471–477. DOI: 10.2494/photopolymer.10.471.

[18] *A model based OPC method to add serifs for corner rounding design of CMOS image sensor.* URL: https://www.spiedigitallibrary.org/conference-proceedings-of-spie/11148/1114813/A-model-based-OPC-method-to-add-serifs-for-corner/10.1117/12.2536495.full (visited on 06/19/2021).

[19] Peter De Bisschop. "How to make lithography patterns print: The role of OPC and pattern layout". In: *Advanced Optical Technologies* 0 (Jan. 20, 2015). DOI: 10.1515/aot-2015-0023.

[20] T. R. Groves et al. "Maskless electron beam lithography: prospects, progress, and challenges". In: *Microelectronic Engineering.* Micro- and Nano-Engineering 2001 61-62 (July 1, 2002), pp. 285–293. ISSN: 0167-9317. DOI: 10.1016/S0167-9317(02)00528-2. URL: https://www.sciencedirect.com/science/article/pii/S0167931702005282 (visited on 06/19/2021).

[21] Daniel Berkoh and Sarang Kulkarni. "Challenges in Lift-Off Process Using CAMP Negative Photoresist in III–V IC Fabrication". In: *IEEE Transactions on Semiconductor Manufacturing* 32.4 (Nov. 2019). Conference Name: IEEE Transactions on Semiconductor Manufacturing, pp. 513–517. ISSN: 1558-2345. DOI: 10.1109/TSM.2019.2944133.

[22] "LOR and PMGI Resists for Bi-layer Lift-off Processing - Technical Datasheet". In: Nov. 2019. URL: https://kayakuam.com/wp-content/uploads/2019/09/KAM-LOR-PMGI-Data-Sheet-11719.pdf (visited on 06/19/2021).

[23] James Cameron et al. "Developable BARC (DBARC) technology as a solution to today's implant lithography challenges". In: *Advances in Resist Materials and Processing Technology XXVIII.* Advances in Resist Materials and Processing Technology XXVIII. Vol. 7972. International Society for Optics and Photonics, Apr. 15, 2011, p. 797214. DOI: 10.1117/12.881614. URL: https://www.spiedigitallibrary.org/conference-proceedings-of-spie/7972/797214/Developable-BARC-DBARC-technology-as-a-solution-to-todays-implant/10.1117/12.881614.short (visited on 06/19/2021).

[24] J. Tallal et al. “4 inch lift-off process by trilayer nanoimprint lithography”. In: *Journal of Vacuum Science & Technology B: Microelectronics and Nanometer Structures Processing, Measurement, and Phenomena* 23.6 (Nov. 1, 2005). Publisher: American Institute of Physics, pp. 2914–2919. ISSN: 1071-1023. DOI: `10.1116/1.2130351`. URL: `https://avs.scitation.org/doi/10.1116/1.2130351` (visited on 06/19/2021).

[25] Dong Kyo Oh et al. “Nanoimprint lithography for high-throughput fabrication of metasurfaces”. en. In: *Frontiers of Optoelectronics* (Apr. 2021). ISSN: 2095-2767. DOI: `10.1007/s12200-021-1121-8`. URL: `https://doi.org/10.1007/s12200-021-1121-8` (visited on 06/19/2021).

A Process Flow 1

Lab : Advanced NEMS Laboratory
Operator Name : Croux Pierre-Jean
Supervisor Name : M. Liffredo – G. Villanueva
Phone : 0799364731
Office : -
E-mail : pierre-jean.croux@epfl.ch

DUV Lithography for VHF resonators

Description of the fabrication project

The aim of the project is in a first step to optimize the fabrication process of reticle for DUV lithography for VHF resonators application. As frequency of resonance depends on the electrode pitch, scale-down of dimentions will increase the operation frequency. In a second step, we will assess the feasibility of a lift-off using DUV stepper technologyfor resist patterning in order to achieve a critical dimension of 150 [nm] for 50 [nm] thick platinum electrodes.

Technologies used *!! remove non-used !!*			
Mask fabrication, SEM, sputtering, evaporation, DUV lithography			
Ebeam litho data - Photolitho masks - Laser direct write data			
Mask #	**Critical Dimension**	**Critical Alignment**	**Remarks**
1	**0.6 um**	First Mask	Reticle for DUV lithography
Substrate Type			
Silicon <100>, Ø100mm, 525um thick, Double Side polished, TTV2, Prime, p type, 1-10 Ohm.cm			

Interconnections and packaging of final device

Thinning/grinding/polishing of the samples is required at some stage of the process.
☑ No ☐ Yes => confirm involved materials with CMi staff

Dicing of the samples is required at some stage of the process.
☑ No ☐ Yes => confirm dicing layout with CMi staff

Wire-bonding of dies, with glob-top protection, is required at the end of the process.
☑ No ☐ Yes => confirm pads design (size, pitch) and involved materials with CMi staff

Lab : Advanced NEMS Laboratory
Operator Name : Croux Pierre-Jean
Supervisor Name : M. Liffredo – G. Villanueva

Phone : 0799364731
Office : -
E-mail : pierre-jean.croux@epfl.ch

Step-by-step process outline

Step	Process description	Cross-section after process
01	**Substrate**: 6" Mask *Mask reticules writing* Machine: Z5 - VPG200	UV laser scan AZ1512 500 nm Cr203 2 nm Cr 90 nm Quartz
02	*Mask reticules processing* Machine: Z6 - Hamatech Mask Processor *Development (diluted AZ 351B)* *Cr wet etching* *resist striping (AZ 400K)* Mask reticules : *CD = 0.6 µm*	CD Cr203 2 nm Cr 90 nm Quartz
03	**Substrate**: Silicon prime wafers, 100/P/DS/1-10 *Photoresist coating + development* Machine: Z1 – Süss Microtech ACS200 Gen3 cluster *Photoresist :* 1. JSR Micro M108Y 2. JSR Micro M35G *Thickness 1: 450 [nm]* *Thickness 2: 1.2 [nm]* *Developer : AZ726 MIF* *Photoresist exposure* Machine: Z5 – ASML PAS 5500/350 C, DUV stepper *Critical Dimension = 150 [nm]*	
04	*SEM Examination*	*150 [nm]*

05	*Surface activation* Machine: Z2–Tepla GigaBatch Settings: 200 [W], 30 [s] *Thin film deposition* Material : *Titanium + Platinum* Machine: Z11 – EVA 760 Z4 – Pfeiffer SPIDER 600 *Titanium Adhesion layer thickness : 10 [nm]* *Platinum Thin film thickness:40 [nm]*	
06	*Lift-off of the photoresist* Machine: Z1 – Plade Solvent Stripping: Remover-1165 (NMP) Ultrasonic bath: Time = … x 5 [min], T° = 70 [°C] Power = …	
07	*SEM Examination* Note: *After the first examination, the wafer will be cleaved to enable profile inspection*	*150 [nm]*

B Process Flow 2

Lab : Advanced NEMS Laboratory	Phone : 0799364731
Operator Name : Croux Pierre-Jean	Office : -
Supervisor Name : M. Liffredo – G. Villanueva	E-mail : pierre-jean.croux@epfl.ch

DUV Lithography for VHF resonators

Description of the fabrication project

The aim of the project is in a first step to optimize the fabrication process of reticle for DUV lithography for VHF resonators application. As frequency of resonance depends on the electrode pitch, scale-down of dimentions will increase the operation frequency. In a second step, we will assess the feasibility of a etching process using DUV stepper technology for resist patterning in order to achieve a critical dimension of 150 [nm] for 50 [nm] thick platinum electrodes.

Technologies used *!! remove non-used !!*			
Mask fabrication, SEM, sputtering, evaporation, DUV lithography			
Ebeam litho data - Photolitho masks - Laser direct write data			
Mask #	**Critical Dimension**	**Critical Alignment**	**Remarks**
1	**0.6 um**	First Mask	Reticle for DUV lithography
Substrate Type			
Silicon <100>, Ø100mm, 525um thick, Double Side polished, TTV2, LPCVD Si3N4 100 nm, p type, 1-10 Ohm.cm			

Interconnections and packaging of final device

Thinning/grinding/polishing of the samples is required at some stage of the process.

☑ No ☐ Yes => confirm involved materials with CMi staff

Dicing of the samples is required at some stage of the process.

☑ No ☐ Yes => confirm dicing layout with CMi staff

Wire-bonding of dies, with glob-top protection, is required at the end of the process.

☑ No ☐ Yes => confirm pads design (size, pitch) and involved materials with CMi staff

Step-by-step process outline

Step	Process description	Cross-section after process
01	**Substrate**: 6" Mask *Mask reticules writing* Machine: Z5 - VPG200	UV laser scan AZ1512 500 nm Cr203 2 nm Cr 90 nm Quartz
02	*Mask reticules processing* Machine: Z6 - Hamatech Mask Processor *Development (diluted AZ 351B)* *Cr wet etching* *resist striping (AZ 400K)* Mask reticules : *CD = 0.6 µm*	CD Cr203 2 nm Cr 90 nm Quartz
03	**Substrate**: Silicon & LPCVD Si3N4 100 nm wafers, 100/P/DS/1-10 *Surface activation* Machine: Z2–Tepla GigaBatch Settings: 200 [W], 30 [s] *Thin film deposition* Material : *Titanium + Platinum* Machine: Z11 – EVA 760 *Titanium Adhesion layer thickness : 10 [nm]* *Platinum Thin film thickness:40 [nm]*	
04	*Photoresist coating + development* Machine: Z1 – Süss Microtech ACS200 Gen3 cluster or Stepper cleantrack *Photoresist :* JSR Micro M108Y (+ BARC in one process) *Thickness : 450 [nm]* *Developer : AZ726 MIF*	

	Photoresist exposure Machine: Z5 – ASML PAS 5500/350 C, DUV stepper *Critical Dimension = 150 [nm]*	
05	*Etching of the platinum layer* Machine: Z2– STS Multiplex ICP Plasma etcher – Chlorine chemistery *Note: In the case were we used a BARC layer, this layer was etch using the Z02 SPTS APS: dielectric plasma etcher – Fluorine chemistery prior the etch of the platinum*	
06	*Stripping of the remaining photoresist* Machine: Z2–Tepla GigaBatch Settings: 200 [W], 5 [min]	
07	*SEM Examination* Note: *After the first examination, the wafer will be cleaved to enable profile inspection*	*150 [nm]*

C Table of measurements

CMi 01058597

VPG Intensity	Stepper Dose	Theoretical linewidth [nm]	Experimental line width [nm]	Experimental gap [nm]	Type of feature	CD Bias [nm]
8	38	350	436.1	261.7	Electrodes 9	0
8	38	350	432.6	240.4	Electrodes 15	0
7.5	38	500	573.5	430.1	Damiers	0
8	38	500	593.3	415.3	Damiers	0
8.5	38	500	540.7	426.9	Damiers	0
9	38	500	677.3	304.8	Damiers	0
9.5	38	500	707	288.1	Damiers	0
10	38	500	630.9	372.8	Damiers	0
10.5	38	500	747.4	269	Damiers	0
11	38	500	739.9	256.1	Damiers	0
11.5	38	500	687.6	269	Damiers	0
8	38	400	473.1	340.4	Damiers	-150
8	38	400	457.8	337.3	Damiers	-100
8	38	400	464.1	327.6	Damiers	-50
8	38	400	506.9	319.2	Damiers	0
8	38	400	508.2	269	Damiers	50
8	30	400	378.4	416.2	Damiers	0
8	32	400	428.7	385.8	Damiers	0
8	34	400	450.1	364.4	Damiers	0
8	36	400	481.9	312.2	Damiers	0
8	38	400	506.9	319.2	Damiers	0
8	40	400	469.3	306	Damiers	0
8	42	400	539.7	278.5	Damiers	0
8	38	300	315.1	266.6	Damiers	-100
8	38	300	328.4	246.3	Damiers	-50
8	38	300	310.1	257.7	Damiers	0
8	38	300	382.3	208.5	Damiers	50
7.5	38	400	467.9	319.1	Damiers	0
8	38	400	506.9	319.2	Damiers	0
8.5	38	400	416	369.8	Damiers	0
7.5	36	400	489.1	279.5	Damiers	0
8	36	400	481.9	312.2	Damiers	0
8.5	36	400	412.8	388.5	Damiers	0
7.5	36	300	358.1	238.7	Damiers	0
8	36	300	328.4	266.8	Damiers	0
7.5	38	300	348.9	246.3	Damiers	0
8	38	300	310.1	257.7	Damiers	0
7.5	40	300	broken	broken	Damiers	0
8	40	300	328.4	225.8	Damiers	0

CMi 01058599

VPG [Intensity:Defocus]	Stepper Dose	Theoretical linewidth [nm]	Experimental line width [nm]	Experimental gap [nm]	Type of feature	CD Bias [nm]
[20.5;-37]	37	350	406.1	270.8	Electrodes 15	0
[20.5;-37]	37	300	399.7	199.8	Damiers	0
[20.5;-37]	37	750	801.2	734.4	Damiers	0

CMi 01058599

VPG [Intensity:Defocus]	Stepper Dose	Theoretical linewidth [nm]	Experimental line width [nm]	Experimental gap [nm]	Type of feature	CD Bias [nm]
[8;-30]	38	300	381.1	235.9	Damiers	0

Mask DT1

VPG Intensity [%]	VPG Defocus [µm]	Theoretical Gap [nm]	Experimental Gap width [nm]	Experimental Cr [nm]	Type of feature	Note
11.5	-30	600	833.8	-	Damiers	
12.5	-30	600	875	-	Damiers	
13.5	-30	600	905.6	-	Damiers	

Mask DT2

VPG Intensity [%]	VPG Defocus [µm]	Theoretical Gap [nm]	Experimental Gap width [nm]	Experimental Cr [nm]	Type of feature	Note
9.5	-30	600	677.8	-	Damiers	
10	-30	600	728.6	-	Damiers	
10.5	-30	600	804.1	-	Damiers	
11	-30	600	805.3	-	Damiers	
11.5	-30	600	854.2	-	Damiers	
12	-30	600	958.4	-	Damiers	
14.5	-30	600	774.8	-	Damiers	outlier
16.5	-30	600	726.2	-	Damiers	outlier
17	-30	600	791	-	Damiers	outlier

CMi 01058600

VPG [Intensity:Defocus]	Stepper Dose	Theoretical linewidth [nm]	Experimental line width [nm]	Experimental gap [nm]	Type of feature	Note
[8;-30]	24	350	507.6	236.9	Electrodes 15	
[8;-30]	26	350	499.3	208	Electrodes 15	
[8;-30]	28	350	424.2	267.1	Electrodes 15	

CMi 01058355

VPG [Intensity:Defocus]	Stepper Dose	Theoretical linewidth [nm]	Experimental line width [nm]	Experimental gap [nm]	Type of feature	Note
[8;-30]	24	350	408	293.8	Electrodes 15	
[8;-30]	26	350	399.4	285.3	Electrodes 15	
[8;-30]	28	350	391.1	313.1	Electrodes 15	
[8;-30]	28	150	190.1	133.1	Electrodes 15	elec touch
[8;-30]	28	200	258.4	193.8	Electrodes 15	good pattern
[8;-30]	28	250	265.1	225.4	Electrodes 15	good pattern

D Budget

STI-IGM-NEMS - 108056 - MA4_J.-P.Croux

Date	Heure	Equipement	Machine					Opérateur		Total
			Fix (CHF/run)	Durée HP (hh:mm)	P.U. HP (CHF/h)	Durée HC (hh:mm)	P.U. HC (CHF/h)	Durée M.O. (hh:mm)	P.U.M.O. (CHF/h)	Montant (CHF)
25.03.21	10:00	E10 - Z01 Zeiss LEO 1550 - Scanning Electron Microscope	12	01:06	18	00:00	18	00:00	63	31.8
26.03.21	10:09	E10 - Z01 Zeiss LEO 1550 - Scanning Electron Microscope	12	00:50	18	00:00	18	00:00	63	27
01.04.21	09:08	E10 - Z01 Zeiss LEO 1550 - Scanning Electron Microscope	12	00:58	18	00:00	18	00:00	63	29.4
15.04.21	08:43	E04 - Z01 ACS200 - Coater and Developer System for Positive Resist	12	00:11	100	00:00	100	00:00	63	30.33
15.04.21	14:00	E01 - Z05 ASML PAS 5500/350C - DUV Stepper	35	00:30	51	00:00	51	00:30	63	92
15.04.21	14:01	E04 - Z01 ACS200 - Coater and Developer System for Positive Resist	12	00:09	100	00:00	100	00:00	63	27
16.04.21	11:59	E11 - Z11 Tepla 300 - Microwave plasma stripper	4	00:13	12	00:00	12	00:00	63	6.6
16.04.21	12:08	E07 - Z11 Alliance-Concept EVA760 - Evaporator	12	00:58	55	00:00	55	00:00	63	65.17
16.04.21	15:19	E09 - Z01 Plade Solvent - Photolithography wet bench	12	00:26	45	00:00	45	00:00	63	31.5
20.04.21	15:29	E10 - Z01 Zeiss LEO 1550 - Scanning Electron Microscope	12	02:18	18	00:00	18	00:00	63	53.4
22.04.21	11:01	E03 - Z05 Heidelberg VPG200 - Laser lithography system	12	00:32	32	00:00	32	00:00	63	29.07
22.04.21	11:56	E04 - Z06 Hamatech Mask Processor	12	00:21	100	00:00	100	00:00	63	47
23.04.21	13:39	E10 - Z01 Zeiss LEO 1550 - Scanning Electron Microscope	12	01:39	18	00:00	18	00:00	63	41.7
23.04.21	15:24	E09 - Z01 Plade Solvent - Photolithography wet bench	12	00:24	45	00:00	45	00:00	63	30
26.04.21	15:15	E03 - Z05 Heidelberg VPG200 - Laser lithography system	12	00:32	32	00:00	32	00:00	63	29.07
26.04.21	16:02	E04 - Z06 Hamatech Mask Processor	12	00:27	100	00:00	100	00:00	63	57
29.04.21	16:23	E03 - Z05 Heidelberg VPG200 - Laser lithography system	12	01:22	32	00:00	32	00:00	63	55.73
29.04.21	17:11	E09 - Z01 Plade Solvent - Photolithography wet bench	12	00:19	45	00:00	45	00:00	63	26.25
11.05.21	10:18	E01 - Z05 ASML PAS 5500/350C - DUV Stepper	35	00:13	51	00:00	51	00:13	63	59.7
11.05.21	11:03	E04 - Z01 ACS200 - Coater and Developer System for Positive Resist	12	00:23	100	00:00	100	00:00	63	50.33
28.05.21	13:29	E07 - Z11 Alliance-Concept EVA760 - Evaporator	12	00:57	55	00:00	55	00:00	63	64.25
28.05.21	13:38	E11 - Z11 Tepla 300 - Microwave plasma stripper	4	00:19	12	00:00	12	00:00	63	7.8
28.05.21	15:45	E09 - Z01 Plade Solvent - Photolithography wet bench	12	00:13	45	00:00	45	00:00	63	21.75
31.05.21	16:24	E09 - Z01 Plade Solvent - Photolithography wet bench	12	00:42	45	00:00	45	00:00	63	43.5
02.06.21	10:01	E09 - Z01 Plade Solvent - Photolithography wet bench	12	00:07	45	00:00	45	00:00	63	17.25
02.06.21	10:13	E04 - Z01 ACS200 - Coater and Developer System for Positive Resist	12	00:24	100	00:00	100	00:00	63	52
02.06.21	11:00	E01 - Z05 ASML PAS 5500/350C - DUV Stepper	35	00:20	51	00:00	51	00:20	63	73
02.06.21	11:22	E09 - Z01 Plade Solvent - Photolithography wet bench	12	00:15	45	00:00	45	00:00	63	23.25
02.06.21	16:33	E09 - Z01 Plade Solvent - Photolithography wet bench	12	00:07	45	00:00	45	00:00	63	17.25
02.06.21	18:12	E09 - Z01 Plade Solvent - Photolithography wet bench	12	00:26	45	00:00	45	00:00	63	31.5
07.06.21	11:05	E10 - Z01 Zeiss LEO 1550 - Scanning Electron Microscope	12	00:58	18	00:00	18	00:00	63	29.4
08.06.21	09:01	E10 - Z01 Zeiss LEO 1550 - Scanning Electron Microscope	12	01:01	18	00:00	18	00:00	63	30.3
09.06.21	16:34	E10 - Z01 Zeiss LEO 1550 - Scanning Electron Microscope	12	01:29	18	00:00	18	00:00	63	38.7
14.06.21	17:04	E10 - Z01 Zeiss LEO 1550 - Scanning Electron Microscope	12	02:01	18	00:00	18	00:00	63	48.3
16.06.21	16:43	E11 - Z02 Tepla GigaBatch - Microwave plasma stripper	4	00:13	12	00:00	12	00:00	63	6.6
16.06.21	16:58	E10 - Z01 Zeiss LEO 1550 - Scanning Electron Microscope	12	01:50	18	00:00	18	00:00	63	45
17.06.21	16:55	E10 - Z01 Zeiss LEO 1550 - Scanning Electron Microscope	12	01:36	18	00:00	18	00:00	63	40.8
24.06.21	14:50	E10 - Z01 Zeiss LEO 1550 - Scanning Electron Microscope	12	01:04	18	00:00	18	00:00	63	31.2
									Total	1441.9

STI-IGM-NEMS - 108056 - MA4_J.-P.Croux

Date	Responsable	Prestation	Quant. (U)	PU (Frs)	PT (Frs)
28.05.21	rjuttin	EVA760 - Pt (450mm) / MA4	63 nm	0.43	27.09
26.05.21	gkumuntu	100/P/DS/0.1-0.5 TTV2 & LPCVD Si3N4 100nm / MA4	2	60.3	120.6
01.04.21	gkumuntu	Box (20 x 7 x 3 cm) for pens, tweezers / MA4	1	8	8
01.04.21	gkumuntu	Wafer tweezers (plastic tip) / MA4	1 pc	27.15	27.15
07.04.21	gkumuntu	100/P/DS/0.1-0.5 TTV2 / MA4	4	49.15	196.6
16.04.21	rjuttin	EVA760 - Pt (450mm) / MA4	63 nm	0.43	27.09
19.04.21	gkumuntu	Quartz Chrome Blank 6" (stepper reticle) / MA4	1 plaque	493.15	493.15
21.04.21	gkumuntu	Chrome Blank 5" / MA4	1 plaque	27.65	27.65
26.04.21	gkumuntu	Chrome Blank 5" / MA4	1 plaque	27.65	27.65
25.03.21	gkumuntu	Cleanroom notebook / MA4	1	6.95	6.95
				Total	961.93
				Total Final	2403.83